Evaluating SCAN and r^{2}SCAN meta-GGA functionals for predicting transition temperatures in antiferromagnetic materials

Nafise Rezaei,[1] Mojtaba Alaei,[1,2] and Artem R. Oganov[1]

[1] *Skolkovo Institute of Science and Technology, 121205, Bolshoy Boulevard 30, bld. 1, Moscow, Russia.*
[2] *Department of Physics, Isfahan University of Technology, Isfahan 84156-83111, Iran.*

(Dated: March 13, 2025)

Recent advancements in exchange-correlation functionals within density functional theory highlight the need for rigorous validation across diverse types of materials properties. In this study, we assess the performance of the newly developed meta-GGA r^{2}SCAN and its predecessor, SCAN, in predicting the Néel transition temperature of antiferromagnetic materials. Our analysis includes 48 magnetic materials, spanning both simple and complex systems. Using DFT, we compute the energies of various magnetic configurations and extract exchange interaction parameters through a least-squares fitting approach. These parameters are then used in classical Monte Carlo simulations to estimate the transition temperatures. Our results demonstrate that both SCAN and r^{2}SCAN greatly outperform standard GGA and GGA+U methods, yielding predictions that closely align with experimental values. The Pearson correlation coefficients for SCAN and r^{2}SCAN are 0.97 and 0.98, respectively, when compared to experimental transition temperatures. Additionally, we calculate the energy differences between antiferromagnetic and ferromagnetic configurations to assess the performance of the hybrid HSE06 functional. We found that the HSE06 functional underestimates transition temperatures compared to the meta-GGA functionals and experimental values.

I. INTRODUCTION

The exchange-correlation (xc) functional is a crucial component of the Kohn-Sham density functional theory (DFT), as it encapsulates the complex many-body effects of electron-electron interactions. The accuracy of DFT calculations heavily depends on the choice of xc functional, especially for magnetic calculations. Magnetism serves as an ideal ground for testing and improving exchange-correlation (xc) functionals, as it directly arises from the presence of xc energy in the many-body Hamiltonian [1, 2].

The local density approximation (LDA) [3] and the generalized gradient approximation (GGA) [4, 5], as commonly used xc functionals, both face challenges in describing systems with strong on-site Coulomb interactions, such as those involving d and f orbitals. These limitations, stemming from self-interaction errors [6], lead to inaccuracies in predicting electronic structures and magnetic properties. For example, LDA often results in incorrect magnetic moments for strongly correlated materials and fails to predict the correct magnetic crystal structures [7]. GGA offers improved accuracy with respect to LDA, providing reasonable predictions for magnetic moments; nevertheless, GGA struggles to open sufficiently band gaps and fully capture strong electronic correlations.

To address these limitations, the GGA+U method [8, 9] was introduced, which adds an on-site Coulomb interaction term to better account for strong electronic correlations. However, the accuracy of GGA+U heavily depends on the U parameter, which must be carefully tuned for each system. Hybrid functionals, which mix a portion of Hartree-Fock exchange with LDA or GGA functionals, offer further improvements in accuracy but are often computationally prohibitive, particularly for large or complex systems. Both GGA+U and hybrid functionals fall into the category of orbital-dependent density functionals [10], where the direct use of orbitals in the Hamiltonian helps to partially correct self-interaction errors. Therefore, it is prudent to also consider other functionals in this category, such as meta-GGA, for studying magnetic materials.

Meta-generalized gradient approximation (meta-GGA) functionals, such as the Strongly Constrained and Appropriately Normed (SCAN) functional [11], represent a significant advancement over traditional functionals [12]. These functionals improve the localization of d-electrons [13], leading to more realistic band gap predictions and addressing many of the limitations associated with both LDA and GGA. The improved d-electron localization enables meta-GGA functionals to better describe magnetic materials that are Mott insulators. However, this feature can also result in an overestimation of magnetic moments in itinerant ferromagnets, such as iron (Fe) [6].

SCAN demonstrates superior performance in magnetic and non-magnetic materials [12, 14] but demands dense real-space grids to mitigate numerical instabilities [15]. This computational demand can pose challenges.

To overcome the instability challenges, the restored regularized SCAN (r^{2}SCAN) functional [15] was developed. This functional retains the accuracy of SCAN while improving numerical stability and computational efficiency [16]. In transition metal oxides, r^{2}SCAN has demonstrated superior performance, balancing accuracy and efficiency, making it an attractive option for studying magnetic systems.

Numerous benchmarks are available for assessing xc functionals in predicting properties such as bond lengths, band gaps, and energy barriers [17]. However, in the field of magnetism, where xc functionals play a criti-

cal role, benchmarking efforts remain limited, particularly for magnetic interactions. Studies on meta-GGA functionals for magnetic materials have highlighted limitations, such as their tendency to overestimate magnetic moments in itinerant ferromagnets, where GGA often yields more accurate results [6, 18, 19]. Other investigations have examined such properties as equilibrium volumes, band gaps for transition metals ($3d$, $4d$, and $5d$)[20], Heusler alloys[12], and transition metal oxides [21], showcasing certain advantages of meta-GGA over GGA. Despite these efforts, a comprehensive study on the prediction of magnetic thermodynamic properties is still lacking. Establishing robust benchmark sets for magnetic materials is crucial to addressing the challenges in DFT calculations for these systems.

In our previous work, we benchmarked the Perdew-Burke-Ernzerhof (PBE) [5] GGA and GGA+U functionals for predicting the transition temperatures of antiferromagnetic (AFM) materials. The results showed that GGA tends to overestimate, while GGA+U tends to underestimate, the exchange coupling interactions [22], leading to correspondingly higher and lower estimates of the Néel transition temperature. These findings highlight the need for improved xc functionals to achieve more accurate predictions of magnetic coupling.

In this study, we aim to evaluate the accuracy of the SCAN and r^{2}SCAN functionals in predicting the transition temperature of insulating AFM materials. To achieve this, we calculate magnetic exchange couplings using total energy calculations for various magnetic configurations with these functionals. These exchange interactions are then used to construct a model Hamiltonian, which is analyzed through Monte Carlo (MC) simulations. We also evaluate how the predicted transition temperature from DFT changes as we advance to higher-level functionals on Jacob's ladder [23], ascending from meta-GGA to hybrid functionals like HSE06.

The paper is organized as follows: In Section II, we describe the computational details for obtaining transition temperatures. Section III presents an analysis of the predicted transition temperatures using SCAN and r^{2}SCAN, including a comparison between the two functionals and with HSE06. The paper concludes with a summary of findings and implications. In the appendix, we provide a table listing the transition temperatures predicted by SCAN and r^{2}SCAN alongside their experimental values. Additionally, the supplementary materials include all exchange parameters obtained from SCAN and r^{2}SCAN for each compound.

II. COMPUTATIONAL DETAILS AND MATERIALS

A. DFT and MC

The experimental structures, including both atomic positions and lattice vectors, are directly used for all *ab initio* calculations. No *ab initio* geometrical optimization is performed on these structures. To determine up to which nth nearest neighbor to include in the calculations, we consider both the distance and the bonding connections between magnetic sites. Distances greater than 7 Å are generally excluded unless there are atomic bond connections with angles close to 180° at such distances. For layered structures, we ensure that the interactions considered include at least one exchange interaction between adjacent layers.

Calculating exchange parameters up to the nth nearest neighbor requires a supercell structure that is mathematically capable of supporting such calculations. This is achieved using the SUPERHEX code [24], which generates optimized supercells specifically designed for determining exchange interactions up to the desired nth nearest neighbor. For most compounds, the generated supercells contain 32 to 84 atoms, although for some structures, the number of atoms was as large as 112.

We perform spin-polarized density functional theory calculations using the Vienna Ab-initio Simulation Package (VASP) [25], employing a plane-wave basis set with an energy cutoff of 600 eV. The Brillouin zone is sampled with a Monkhorst-Pack grid, maintaining a k-point spacing of 0.15 Å^{-1}. To address convergence challenges in meta-GGA calculations, we initialize each magnetic configuration using wave functions and charge densities obtained from converged GGA or GGA+U calculations. We use the PBE xc functional for both GGA and GGA+U calculations.

To estimate exchange interactions, we map the DFT results onto the Heisenberg Hamiltonian [22, 26]:

$$\hat{\mathcal{H}} = -\frac{1}{2}\sum_{i,j} J_{ij}\hat{\mathbf{S}}_i \cdot \hat{\mathbf{S}}_j,$$

where $\hat{\mathbf{S}}_i$ and $\hat{\mathbf{S}}_j$ are unit magnetic vectors at sites i and j, and J_{ij} represents the coupling constants.

To determine the Heisenberg exchange interactions using the total energy [22, 26], at least $n+1$ magnetic configurations are required to calculate coupling constants up to the *nth* nearest neighbors. However, small induced magnetic moments often appear on non-magnetic atoms, which can affect the results. To improve accuracy, it is recommended to use more magnetic configurations than the minimal requirement [27]. The least-squares method is applied to fit the energy differences between magnetic configurations to evaluate exchange interactions.

For each compound, we use at least three times the minimal number of magnetic configurations and monitor the convergence of the coupling constants as the number of configurations increases. If convergence is unsatisfactory, we add more configurations until a satisfactory result is achieved.

To compute the Néel temperature, we utilize the ESpinS code [28], which performs classical MC calculations based on the Heisenberg Hamiltonian. We select supercells containing at least 2000 magnetic atoms per cell.

This choice ensures adequate sampling of magnetic interactions and minimizes finite-size effects. We execute 10^6 MC steps for thermalization and 10^6 steps for sampling, collecting data every 5 steps. When large fluctuations are observed, the thermalization steps are increased to 2×10^6 and the sampling steps to 3×10^6 to enhance accuracy. To accelerate convergence to stable configurations, we employ the parallel tempering method, exchanging configurations every 10 MC steps.

B. MATERIALS

In this study, we investigate a total of 48 AFM materials, including 27 of the 29 compounds from our previous work using GGA and GGA+U methods [22]. Among the previously selected compounds, we encountered convergence issues in the total energy calculations for $LiCoPO_4$ when using the SCAN and r^{2}SCAN functionals. Also, we exclude KMnSb from this study, which was included in our previous work, because we found no definitive experimental reports on its transition temperature.

We limit our selection to $3d$ magnetic materials to avoid additional complexities arising from spin-orbit coupling. Additionally, we focus on insulating magnetic materials to avoid itinerant magnetism, which typically requires accounting for exchange interactions over very long distances. The selected materials, along with references to their experimental structures, are as follows: YVO_3 [29], $CrSb_2$ [30], $CrCl_2$ [31], CrF_2 [32], Cr_2O_3 [33], CrSBr [34], Cr_2TeO_6 [35], Cr_2WO_6 [35], MnO [36], MnS [37], MnSe [38], MnTe [39], MnO_2 [40], MnF_2 [41], MnS_2 [42],$MnTe_2$ [43], $LiMnO_2$ [44], $SrMnO_3$ [45], $KMnF_3$ [46], $MnPS_3$ [47], $MnPSe_3$ [48], $MnWO_4$ [49], Li_2MnO_3 [50], $LiMnPO_4$ [51], Fe_2O_3 [52], $SrFeO_2$ [53], $BiFeO_3$ [54], $LaFeO_3$ [55], $YFeO_3$ [56], $FePS_3$ [57], Fe_2TeO_6 [35], $SrFe_2S_2O$ [58], $CoWO_4$ [59], NiO [60], NiF_2 [61], $NiBr_2$ [62], NiS_2 [63], $NiCl_2$ [64], $NiPS_3$ [65], $NiPSe_3$ [66], $KNiF_3$ [67], $NiWO_4$ [68], La_2NiO_4 [69], K_2NiF_4 [70], $KNiPO_4$ [71], $LiNiPO_4$ [72], CuO [73], CuF_2 [74].

III. RESULTS AND DISCUSSIONS

A. Exchange parameters

We initially validated the reliability of our calculations by employing the PBE PAW potentials in conjunction with the SCAN functional. To ensure accuracy, we selected a series of simple materials, including $CrCl_2$, Cr_2O_3, MnO, MnS, MnSe, MnF_2, NiO, and NiF_2, computed their magnetic exchange couplings using the FHI-aims program package [75]. A comparison between the results obtained from FHI-aims and VASP packages, presented in Table I, demonstrates compatibility between the two codes, confirming that the meta-GGA functional can be reliably used with these pseudo-potentials.

Theoretically, obtaining Heisenberg exchange interactions up to the nth nearest neighbor requires a minimum of $n+1$ unique magnetic configurations. However, practical considerations introduce additional challenges, such as the induced magnetic moments of anions like oxygen atoms. To address these complexities, it is advisable to utilize a greater number of magnetic configurations and to determine the Heisenberg exchanges using the least-squares method, as suggested in our previous work [27]. Consequently, we employ approximately three times the minimum required number of magnetic configurations to account for these additional factors and enhance the accuracy of our results.

The exchange constants for most compounds converge when only a few additional configurations beyond the minimal set are included. Figure 1 (a) illustrates the variation of J_2 for NiO and J_5 for CuO as a function of the number of magnetic configurations. For both compounds, adding just 3 to 4 configurations beyond the minimal set is generally sufficient to achieve convergence.

For NiO, the minimal set of configurations yields a J_2 value that is reasonably close to the converged result. In contrast, for CuO, the minimal configurations result in a J_5 value that deviates significantly from the converged value. This demonstrates that relying solely on the minimal configuration set to calculate exchange interactions can lead to substantial inaccuracies.

We encounter convergence challenges when studying compounds that exhibit metallic band structure in certain magnetic configurations. In contrast, insulating configurations tend to converge more readily. To ensure reliable convergence of exchange interactions, we exclude metallic magnetic configurations from our analysis. Figure 1 (b) illustrates how J_1 for MnTe fails to converge properly when all 34 magnetic configurations, including metallic ones, are considered. However, by excluding two

Compound	$J_{\mathrm{SCAN(VASP)}}$ (meV)	$J_{\mathrm{SCAN(FHI\text{-}aims)}}$ (meV)
$CrCl_2$	$J_1 = -5.15$	$J_1 = -5.30$
	$J_2 = 0.08$	$J_2 = -0.27$
Cr_2O_3	$J_1 = -29.21$	$J_1 = -28.04$
	$J_2 = -17.63$	$J_2 = -18.39$
MnO	$J_1 = -7.85$	$J_1 = -7.27$
	$J_2 = -10.13$	$J_2 = -10.28$
MnS	$J_1 = -2.00$	$J_1 = -1.49$
	$J_2 = -13.79$	$J_2 = -13.51$
MnSe	$J_2 = -13.31$	$J_2 = -11.21$
	$J_4 = -2.64$	$J_4 = -1.89$
MnF_2	$J_1 = 0.34$	$J_1 = -0.45$
	$J_2 = -4.07$	$J_2 = -3.96$
NiO	$J_1 = 2.29$	$J_1 = 2.40$
	$J_2 = -28.30$	$J_2 = -27.37$
NiF_2	$J_1 = -0.80$	$J_1 = -0.40$
	$J_2 = -3.84$	$J_2 = -3.77$

TABLE I. Comparison of the two largest exchange coupling interactions for each material calculated using VASP and FHI-aims packages.

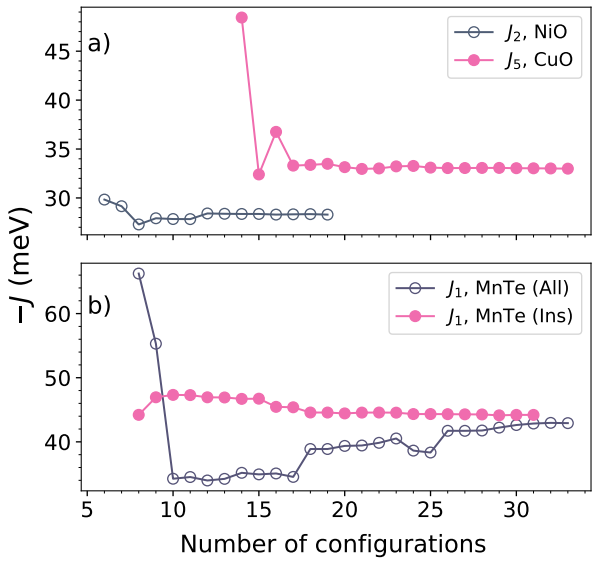

FIG. 1. The plots illustrate the convergence behavior of exchange parameters as a function of the number of magnetic configurations. Plot (a) shows the convergence of the largest exchange parameters for NiO (J_2) and CuO (J_5). Plot (b) highlights the impact of including versus excluding metallic configurations on the convergence of J_1 for MnTe. "All" refers to data including both metallic and insulating configurations, while "Ins" refers to data derived exclusively from insulating configurations.

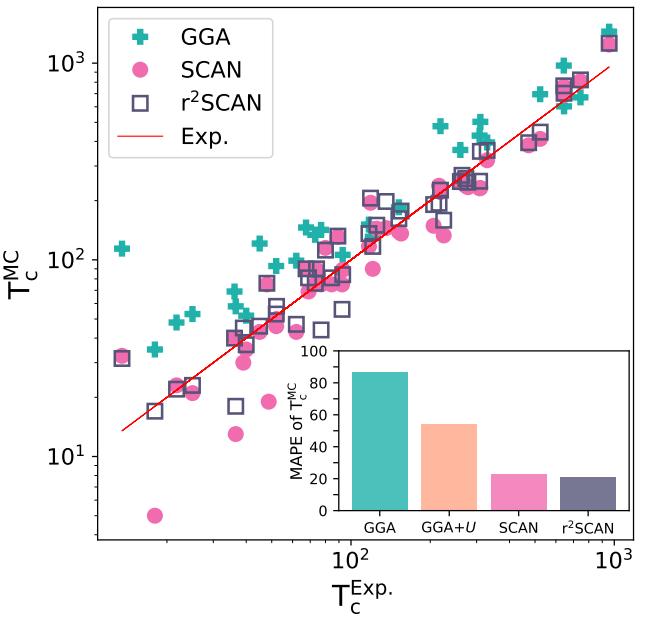

FIG. 2. A comparison of computed Néel transition temperatures in SCAN and r^{2}SCAN functional from MC simulations with experimental transition temperatures. Inset figure represents the total mean absolute percentage error (MAPE) of transition temperatures in different functional. The GGA and GGA+U data are taken from ref [22].

metallic configurations, J_1 converges significantly faster to a stable value.

AFM ordering is observed in the exchange interaction couplings of all studied compounds, except for CrF_2, where the r^{2}SCAN functional predicts ferromagnetic (FM) ordering. The exchange parameters obtained from SCAN and r^{2}SCAN functionals are given in the Supplemental material [76].

B. SCAN and r^{2}SCAN transition temperature

Figure 2 compares the transition temperatures obtained from MC simulations using the SCAN and r^{2}SCAN meta-GGA functionals with experimental transition temperatures. The predictions from both SCAN and r^{2}SCAN functionals show variations, sometimes overestimating and sometimes underestimating the experimental values. However, overall, the transition temperatures computed with these meta-GGA functionals align significantly better with experimental data compared to those obtained using GGA and GGA+U methods.

The mean absolute percentage error (MAPE) is 23% for SCAN functional and 22% for r^{2}SCAN functional, demonstrating their superior accuracy. In comparison, GGA and GGA+U functionals exhibit significantly higher MAPE values of 87% and 54% , respectively, as shown in the inset of Figure 2 (the GGA and GGA+U data are taken from our previous work [22], where we used Dudarev's formulation for GGA+U [77]. The Hubbard U parameter was determined using the constrained DFT (cDFT) approach, implemented via density functional perturbation theory (DFPT) [78, 79]). The high Pearson correlation coefficients of 97% for SCAN and 98% for r^{2}SCAN suggest that r^{2}SCAN functional is well-suited for high-throughput calculations. When combined with machine learning techniques, it can enhance the prediction of transition temperatures.

Errors of the calculated transition temperatures for each material is illustrated in Figure 3. A total of 32 materials in the SCAN functional and 35 materials in the r^{2}SCAN functional exhibit errors of less than 25%. The maximum errors are observed for $MnWO_4$, $FePS_3$, CrF_4, and MnS_2, with values of approximately 141 (133)%, 64 (73)%, 61 (not applicable for r^{2}SCAN functional due to incorrect prediction of ferromagnetic (FM) ordering instead of AFM), and 56 (59)%, respectively, for SCAN (r^{2}SCAN) functional.

To evaluate the consistency between the SCAN and r^{2}SCAN functionals in predicting Néel transition temperatures, we analyze the ratio $T_C^{SCAN}/T_C^{r^2SCAN}$. The frequency distribution of these ratios is shown in the inset of Figure 3. A ratio close to 1 indicates strong agreement between the two functionals. For most com-

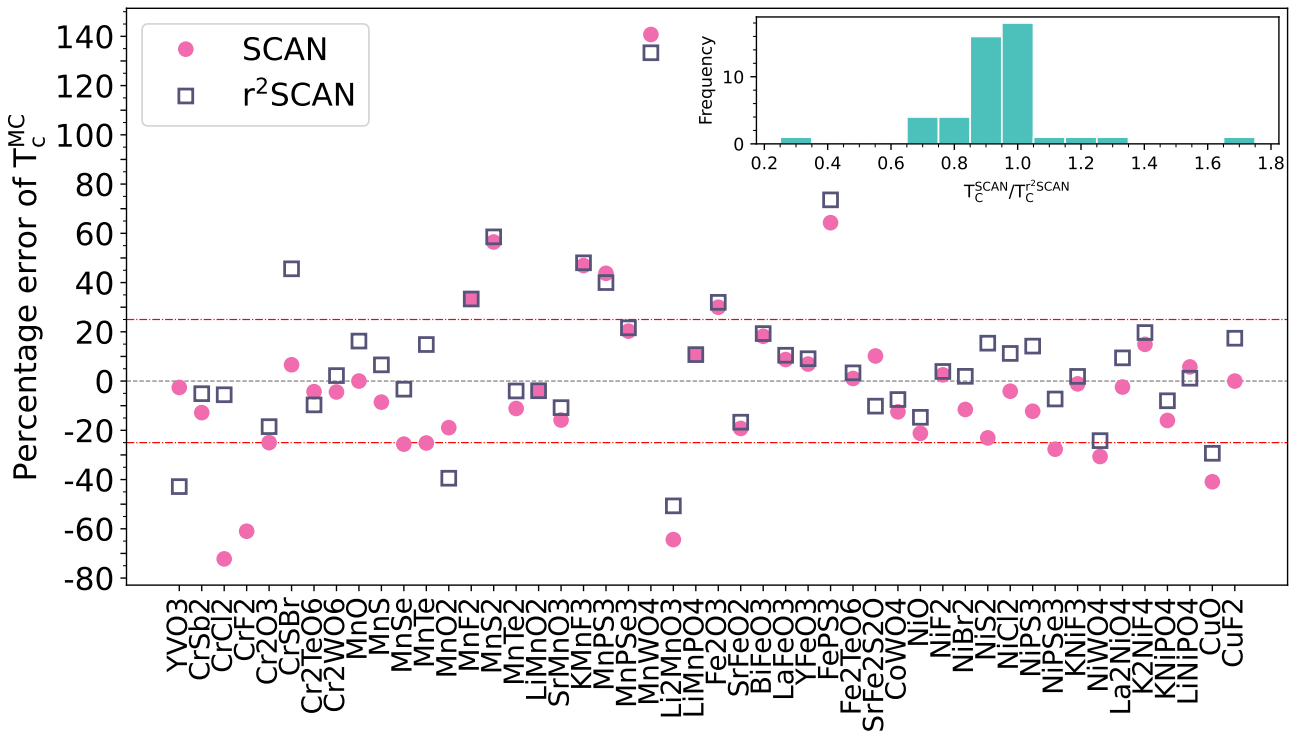

FIG. 3. Percentage error of transition temperatures calculated using MC simulations (T_c^{MC}) with SCAN and r^{2}SCAN functionals across various compounds. For CrF_2, r^{2}SCAN data is excluded as it incorrectly predicts CrF_2 to be FM. Inset of figure represents the frequency distribution of ratio $T_C^{SCAN}/T_C^{r^2SCAN}$.

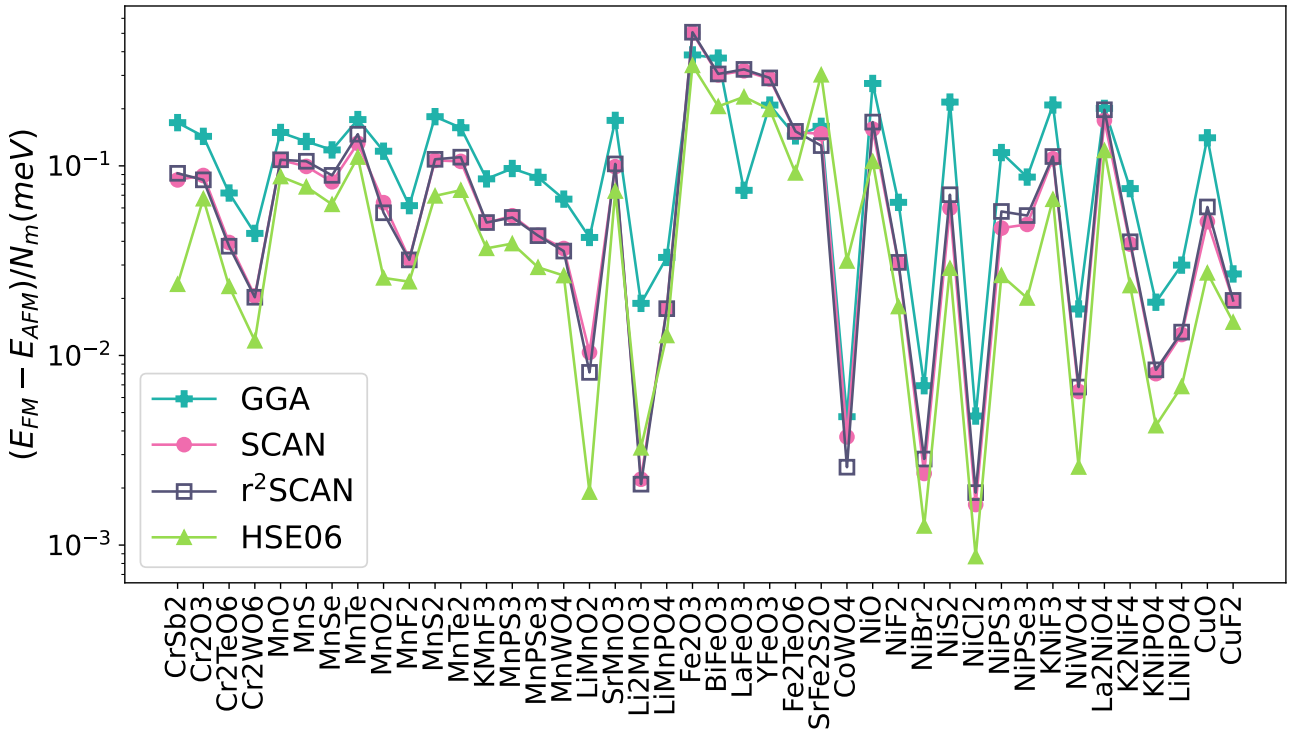

FIG. 4. Energy differences per magnetic atom between AFM and FM configurations for various compounds, calculated using four exchange-correlation functionals: GGA, HSE06, SCAN, and r^{2}SCAN.

pounds (77%), the transition temperatures predicted by SCAN are lower than those predicted by r^{2}SCAN. However, the distribution is centered around 1, indicating that the two functionals generally provide comparable predictions. Deviations from this ratio reflect differences in how the functionals treat specific magnetic systems, likely due to their distinct parameterizations and underlying approximations. In some cases, such as MnTe, the deviation is significant. SCAN functional predicts a transition temperature of 232 K, while r^{2}SCAN functional predicts 356 K, resulting in a difference of 124 K (see Table II).

C. HSE06 functional versus SCAN and r^{2}SCAN functionals

We analyze the energy differences between FM and AFM configurations using the SCAN and r^{2}SCAN functionals, comparing them with results from the GGA and HSE06 functionals. These energy differences reflect the strength of exchange interactions and provide insights into how various *ab initio* methods predict magnetic transition temperatures.

Calculations are conducted on supercells containing two to four magnetic sites. While many of these supercells represent magnetic structures, some compounds require magnetic structures with more than four magnetic sites, rendering HSE06 calculations computationally prohibitive. Consequently, using these smaller supercells (with two to four magnetic sites) instead of magnetic unit cells led some calculations to incorrectly predict ferromagnetism as the stable configuration for certain compounds. To maintain consistency and accuracy, we exclude these cases from the analysis in this subsection. For supercells with four magnetic sites, we select the AFM configurations with the lowest energy among all possible AFM arrangements.

To reduce the computational cost of HSE06 calculations, the energy cutoff was set to 550 eV. As shown in Figure 4, for most compounds, the energy differences per magnetic site predicted by SCAN and r^{2}SCAN functionals fall between those predicted by GGA and HSE06 functionals. GGA functional predicts larger energy differences, indicating stronger exchange coupling and higher transition temperatures for AFM materials. In contrast, HSE06 functional predicts smaller energy differences, suggesting weaker exchange interactions and lower transition temperatures. Since SCAN functional underestimates transition temperatures for nearly half of the compounds, HSE06 is expected to underestimate them even further in these cases. This highlights potential limitations of HSE06 functional for certain materials and underscores the need for continued development of DFT for magnetic systems.

The energy difference between AFM and FM configurations is a key metric for understanding exchange interactions. To improve the reliability of this metric, advanced wavefunction-based methods, such as coupled-cluster singles and doubles (CCSD) or quantum MC simulations, are needed. Data from these methods would be invaluable for refining DFT functionals and enhancing their predictive accuracy for magnetic materials.

IV. CONCLUSIONS

In this study, we evaluated the performance of SCAN and r^{2}SCAN meta-GGA functionals in predicting the Néel transition temperatures of 48 AFM materials. Using a combination of DFT calculations, exchange parameter fitting, and MC simulations, we showed that both SCAN and r^{2}SCAN greatly outperform standard GGA and GGA+U methods in aligning theoretical predictions with experimental data. These findings underscore the potential of meta-GGA functionals as reliable tools for studying magnetic phase transitions, marking a significant step toward more accurate modeling of complex magnetic systems. Although SCAN and r^{2}SCAN generally produce very similar results, our study reveals a significant discrepancy for CrF_2. SCAN correctly identifies the system as AFM, whereas r^{2}SCAN incorrectly predicts it to be FM. Additionally, for cases like MnTe, there is a notable difference between SCAN and r^{2}SCAN in predicting the transition temperature. Although SCAN and r^{2}SCAN have shown significant success in predicting transition temperatures compared to GGA, our calculations faced a major challenge in achieving convergence during the DFT self-consistent cycles when applied to supercell structures. To address this issue, we initialized all calculations with results from GGA or GGA+U. While this approach partially mitigates the problem, it highlights a critical limitation that could hinder the broader application of meta-GGA functionals in magnetic material studies. We also presented a method for analyzing how the hybrid functional HSE06 predicts the transition temperature in comparison to meta-GGA functionals. Our findings suggest that HSE06 underestimates the transition temperature relative to meta-GGA functionals and to experiment.

V. ACKNOWLEDGMENT

This work has been supported by the Russian Science Foundation (Grant 19-72-30043).

Appendix A: Table of transition temperatures

TABLE II. Néel temperature predicted by MC simulations using exchange parameters from SCAN and r^{2}SCAN functionals compared to experimental values.

Compound	T_C^{SCAN} (K)	$T_C^{r^2SCAN}$ (K)	$T_C^{exp.}$ (K)
YVO_3	75	44	77 [80]
$CrSb_2$	238	259	273 [81, 82]
$CrCl_2$	5	17	16, 20 [83–85]
CrF_2	19	–	48.7 [86]
Cr_2O_3	231	251	308 [87–89]
CrSBr	145	198	140, 132 [34, 90]
Cr_2TeO_6	89	84	93 [91]
Cr_2WO_6	43	46	45 [91]
MnO	117	136	117 [92]
MnS	139	162	152 [37]
MnSe	90	117	120, 122 [93, 94]
MnTe	232	356	310 [95, 96]
MnO_2	75	56	92, 93 [97, 98]
MnF_2	90	90	67.3, 67.7 [99, 100]
MnS_2	75	76	48.2, 47.7, 47.9 [101–103]
$MnTe_2$	75	81	86.5, 83.8, 83 [43, 103, 104]
$LiMnO_2$	250	250	261.5, 259 [105, 106]
$SrMnO_3$	234	248	278 [45, 107]
$KMnF_3$	131	132	86.8, 88, 88.2, 89, 95 [46, 100, 108–111]
$MnPS_3$	115	112	82, 78 [112, 113]
$MnPSe_3$	89	90	74 [112, 114]
$MnWO_4$	32.5	31.5	13.5 [49]
Li_2MnO_3	13	18	36.5 [50]
$LiMnPO_4$	40	40	34.8, 34, 36, 42, 33.8 [115–118]
Fe_2O_3	1243	1262	946, 953, 960, 966 [119–123]
$SrFeO_2$	382	394	473 [53]
$BiFeO_3$	760	767	643 [124, 125]
$LaFeO_3$	809	822	738, 750 [126, 127]
$YFeO_3$	689	703	644.5 [128]
$FePS_3$	195	206	117, 116, 123 [112, 113, 129]
Fe_2TeO_6	221	226	201, 233, 206.5, 244, 209 [130–132]
$SrFe_2S_2O$	238	194	216 [133]
$CoWO_4$	35	37	40 [134]
NiO	412	446	523 [135]
NiF_2	75	76	73, 73.3 [136, 137]
$NiBr_2$	46	53	52 [138]
NiS_2	30	45	39 [63]
$NiCl_2$	50	58	52, 52.3 [139, 140]
$NiPS_3$	136	177	155 [112, 113]
$NiPSe_3$	149	191	206 [112]
$KNiF_3$	261	269	275, 253 [67, 108–110]
$NiWO_4$	43	47	62 [141]
La_2NiO_4	321	360	330, 328 [69, 142]
K_2NiF_4	144	150	97.23, 98.7, 180 [143–145]
$KNiPO_4$	21	23	25 [71, 146]
$LiNiPO_4$	23	22	21.8, 21.7 [147, 148]
CuO	133	159	220,225,230 [73, 149, 150]
CuF_2	69	81	69 [151]

[1] F. Illas, I. de P. R. Moreira, J. M. Bofill, and M. Filatov, Extent and limitations of density-functional theory in describing magnetic systems, Phys. Rev. B **70**, 132414 (2004).

[2] A. J. Cohen, P. Mori-Sánchez, and W. Yang, Insights into current limitations of density functional theory, Science **321**, 792 (2008).

[3] J. P. Perdew and A. Zunger, Self-interaction correction to density-functional approximations for many-electron systems, Phys. Rev. B **23**, 5048 (1981).

[4] D. C. Langreth and J. P. Perdew, Theory of nonuniform electronic systems. I. Analysis of the gradient approximation and a generalization that works, Phys. Rev. B **21**, 5469 (1980).

[5] J. P. Perdew, K. Burke, and M. Ernzerhof, Generalized Gradient Approximation Made Simple, Phys. Rev. Lett. **77**, 3865 (1996).

[6] F. Tran, G. Baudesson, J. Carrete, G. K. H. Madsen, P. Blaha, K. Schwarz, and D. J. Singh, Shortcomings of meta-GGA functionals when describing magnetism, Phys. Rev. B **102**, 024407 (2020).

[7] J.-H. Cho and M. Scheffler, Ab initio pseudopotential study of fe, co, and ni employing the spin-polarized lapw approach, Phys. Rev. B **53**, 10685 (1996).

[8] V. I. Anisimov, J. Zaanen, and O. K. Andersen, Band theory and Mott insulators: Hubbard U instead of Stoner I, Phys. Rev. B **44**, 943 (1991).

[9] V. I. Anisimov, F. Aryasetiawan, and A. I. Lichtenstein, First-principles calculations of the electronic structure and spectra of strongly correlated systems: the LDA+ U method, Journal of Physics: Condensed Matter **9**, 767 (1997).

[10] S. Kümmel and L. Kronik, Orbital-dependent density functionals: Theory and applications, Rev. Mod. Phys. **80**, 3 (2008).

[11] J. Sun, A. Ruzsinszky, and J. P. Perdew, Strongly Constrained and Appropriately Normed Semilocal Density Functional, Phys. Rev. Lett. **115**, 036402 (2015).

[12] V. Sokolovskiy, D. Baigutlin, O. Miroshkina, and V. Buchelnikov, Meta-GGA SCAN Functional in the Prediction of Ground State Properties of Magnetic Materials: Review of the Current State, Metals **13**, 10.3390/met13040728 (2023).

[13] D. Hait and M. Head-Gordon, Delocalization Errors in Density Functional Theory Are Essentially Quadratic in Fractional Occupation Number, The Journal of Physical Chemistry Letters **9**, 6280 (2018).

[14] A. D. Kaplan, M. Levy, and J. P. Perdew, The Predictive Power of Exact Constraints and Appropriate Norms in Density Functional Theory, Annual Review of Physical Chemistry **74**, 193 (2023).

[15] J. W. Furness, A. D. Kaplan, J. Ning, J. P. Perdew, and J. Sun, Accurate and Numerically Efficient r2SCAN Meta-Generalized Gradient Approximation, The Journal of Physical Chemistry Letters **11**, 8208 (2020), pMID: 32876454.

[16] R. Kingsbury, A. S. Gupta, C. J. Bartel, J. M. Munro, S. Dwaraknath, M. Horton, and K. A. Persson, Performance comparison of r^2SCAN and SCAN metaGGA density functionals for solid materials via an automated, high-throughput computational workflow, Phys. Rev. Mater. **6**, 013801 (2022).

[17] A. J. Cohen, P. Mori-Sánchez, and W. Yang, Challenges for Density Functional Theory, Chemical Reviews **112**, 289 (2012), pMID: 22191548.

[18] D. Mejía-Rodríguez and S. B. Trickey, Analysis of overmagnetization of elemental transition metal solids from the SCAN density functional, Phys. Rev. B **100**, 041113 (2019).

[19] Y. Fu and D. J. Singh, Density functional methods for the magnetism of transition metals: SCAN in relation to other functionals, Phys. Rev. B **100**, 045126 (2019).

[20] H. Liu, X. Bai, J. Ning, Y. Hou, Z. Song, A. Ramasamy, R. Zhang, Y. Li, J. Sun, and B. Xiao, Assessing r2SCAN meta-GGA functional for structural parameters, cohesive energy, mechanical modulus, and thermophysical properties of 3d, 4d, and 5d transition metals, The Journal of Chemical Physics **160**, 024102 (2024).

[21] S. Swathilakshmi, R. Devi, and G. Sai Gautam, Performance of the r2SCAN Functional in Transition Metal Oxides, Journal of Chemical Theory and Computation **19**, 4202 (2023), pMID: 37329316.

[22] Z. Mosleh and M. Alaei, Benchmarking density functional theory on the prediction of antiferromagnetic transition temperatures, Phys. Rev. B **108**, 144413 (2023).

[23] J. P. Perdew and K. Schmidt, Jacob's ladder of density functional approximations for the exchange-correlation energy, AIP Conference Proceedings **577**, 1 (2001).

[24] M. Alaei and A. R. Oganov, Optimizing Supercell Structures for Heisenberg Exchange Interaction Calculations (2024), arXiv:2410.14356 [cond-mat.mtrl-sci].

[25] G. Kresse and D. Joubert, From ultrasoft pseudopotentials to the projector augmented-wave method, Phys. Rev. B **59**, 1758 (1999).

[26] N. Rezaei, T. Hashemifar, M. Alaei, F. Shahbazi, S. J. Hashemifar, and H. Akbarzadeh, Ab initio investigation of magnetic ordering in the double perovskite Sr_2NiWO_6, Phys. Rev. B **99**, 104411 (2019).

[27] M. Alaei and H. Karimi, A deep investigation of NiO and MnO through the first principle calculations and Monte Carlo simulations, Electronic Structure **5**, 025001 (2023).

[28] N. Rezaei, M. Alaei, and H. Akbarzadeh, ESpinS: A program for classical Monte-Carlo simulations of spin systems, Computational Materials Science **202**, 110947 (2022).

[29] G. R. Blake, T. T. M. Palstra, Y. Ren, A. A. Nugroho, and A. A. Menovsky, Neutron diffraction, x-ray diffraction, and specific heat studies of orbital ordering in YVO_3, Phys. Rev. B **65**, 174112 (2002).

[30] A. Kjekshus, P. G. Peterzens, T. Rakke, and A. F. Andresen, Compounds with the marcasite type crystal structure. XIII. Structural and magnetic properties of $Cr_tFe_{1-t}As_2$, $Cr_tFe_{1-t}Sb_2$, $Fe_{1-t}Ni_tAs_2$, and $Fe_{1-t}Ni_tSb_2$, Acta Chemica Scandinavica A **33**, 469 (1979).

[31] J. W. Tracy, N. Gregory, E. Lingafelter, J. Dunitz, H.-C. Mez, R. Rundle, C. Scheringer, H. Yakel, and M. Wilkinson, The crystal structure of chromium (II) chloride, Acta Crystallographica **14**, 927 (1961).

[32] R. W. G. Wyckoff, *Crystal Structures*, 2nd ed. (Interscience Publishers, New York, 1963).

[33] Refinement of the α Al2O3, Ti2O3, V2O3 and Cr2O3 structures*, Zeitschrift für Kristallographie **117**, 235 (1962).

[34] S. A. López-Paz, Z. Guguchia, V. Y. Pomjakushin, *et al.*, Dynamic magnetic crossover at the origin of the hidden-order in van der Waals antiferromagnet CrSBr, Nature Communications **13**, 4745 (2022).

[35] W. Kunnmann, S. La Placa, L. Corliss, J. Hastings, and E. Banks, Magnetic structures of the ordered trirutiles Cr2WO6, Cr2TeO6 and Fe2TeO6, Journal of Physics and Chemistry of Solids **29**, 1359 (1968).

[36] J. Zhang, Room-temperature compressibilities of MnO and CdO: further examination of the role of cation type in bulk modulus systematics, Physics and Chemistry of Minerals **26**, 644 (1999).

[37] J. K. Clark, V. Yannello, A. M. Samarakoon, C. Ross, M. C. Uible, V. O. Garlea, and M. Shatruk, Inelastic Neutron Scattering Study of Magnetic Exchange Pathways in MnS, The Journal of Physical Chemistry C **125**, 16183 (2021).

[38] Q. Peng, Y. Dong, Z. Deng, H. Kou, S. Gao, and Y. Li, Selective Synthesis and Magnetic Properties of α-MnSe and MnSe2 Uniform Microcrystals, The Journal of Physical Chemistry B **106**, 9261 (2002).

[39] F. Grønvold, N. J. Kveseth, F. D. S. Marques, and J. Tichy, Thermophysical properties of manganese monotelluride from 298 to 700 K. Lattice constants, magnetic susceptibility, and antiferromagnetic transition, The Journal of Chemical Thermodynamics **4**, 795 (1972).

[40] Y. D. Kondrashev and A. Zaslavskii, The structure of the modifications of manganese (IV) oxide, Izvestiya Akademii Nauk SSSR, Seriya Fizicheskaya **15**, 179 (1951).

[41] X. Li, J. Lu, G. Peng, L. Jin, and S. Wei, Solvothermal synthesis of MnF2 nanocrystals and the first-principle study of its electronic structure, Journal of Physics and Chemistry of Solids **70**, 609 (2009).

[42] X-ray and neutron diffraction study of the crystal structure of MnS2, Zeitschrift für Kristallographie - Crystalline Materials **199**, 13 (1992).

[43] P. Burlet, E. Ressouche, B. Malaman, R. Welter, J. P. Sanchez, and P. Vulliet, Noncollinear magnetic structure of $MnTe_2$, Phys. Rev. B **56**, 14013 (1997).

[44] V. Galakhov, M. Korotin, N. Ovechkina, E. Kurmaev, V. Gorshkov, D. Kellerman, S. Bartkowski, and M. Neumann, Electronic structure of LiMnO: X-ray emission and photoelectron spectra and band structure calculations, The European Physical Journal B - Condensed Matter and Complex Systems **14**, 281 (2000).

[45] A. Daoud-Aladine, C. Martin, L. C. Chapon, M. Hervieu, K. S. Knight, M. Brunelli, and P. G. Radaelli, Structural phase transition and magnetism in hexagonal $SrMnO_3$ by magnetization measurements and by electron, x-ray, and neutron diffraction studies, Phys. Rev. B **75**, 104417 (2007).

[46] K. S. Knight, D. D. Khalyavin, P. Manuel, C. L. Bull, and P. McIntyre, Nuclear and magnetic structures of KMnF3 perovskite in the temperature interval 10 K–105 K, Journal of Alloys and Compounds **842**, 155935 (2020).

[47] E. Ressouche, M. Loire, V. Simonet, R. Ballou, A. Stunault, and A. Wildes, Magnetoelectric $MnPS_3$ as a candidate for ferrotoroidicity, Phys. Rev. B **82**, 100408 (2010).

[48] S. Calder, A. V. Haglund, A. I. Kolesnikov, and D. Mandrus, Magnetic exchange interactions in the van der Waals layered antiferromagnet $MnPSe_3$, Phys. Rev. B **103**, 024414 (2021).

[49] G. Lautenschläger, H. Weitzel, T. Vogt, R. Hock, A. Böhm, M. Bonnet, and H. Fuess, Magnetic phase transitions of $MnWO_4$ studied by the use of neutron diffraction, Phys. Rev. B **48**, 6087 (1993).

[50] P. Strobel and B. Lambert-Andron, Crystallographic and magnetic structure of Li2MnO3, Journal of Solid State Chemistry **75**, 90 (1988).

[51] S. Geller and J. L. Durand, Refinement of the structure of $LiMnPO_4$, Acta Crystallographica **13**, 325 (1960).

[52] L. Pauling and S. B. Hendricks, THE CRYSTAL STRUCTURES OF HEMATITE AND CORUNDUM, Journal of the American Chemical Society **47**, 781 (1925).

[53] Y. Tsujimoto, C. Tassel, N. Hayashi, T. Watanabe, H. Kageyama, K. Yoshimura, M. Takano, M. Ceretti, C. Ritter, and W. Paulus, Infinite-layer iron oxide with a square-planar coordination, Nature **450**, 1062 (2007).

[54] S. M. Selbach, M.-A. Einarsrud, T. Tybell, and T. Grande, Synthesis of BiFeO3 by Wet Chemical Methods, Journal of the American Ceramic Society **90**, 3430 (2007).

[55] L. Sangaletti, L. E. Depero, B. Allieri, P. Nunziante, and E. Traversa, An X-ray study of the trimetallic LaxSm1-xFeO3 orthoferrites, Journal of the European Ceramic Society **21**, 719 (2001).

[56] D. du Boulay, E. N. Maslen, V. A. Streltsov, and N. Ishizawa, A synchrotron X-ray study of the electron density in $YFeO_3$, Acta Crystallographica Section B **51**, 921 (1995).

[57] D. Lançon, H. C. Walker, E. Ressouche, B. Ouladdiaf, K. C. Rule, G. J. McIntyre, T. J. Hicks, H. M. Rønnow, and A. R. Wildes, Magnetic structure and magnon dynamics of the quasi-two-dimensional antiferromagnet $FePS_3$, Phys. Rev. B **94**, 214407 (2016).

[58] H. Guo, M.-T. Fernández-Díaz, A. C. Komarek, S. Huh, P. Adler, and M. Valldor, Long-Range Antiferromagnetic Order on Spin Ladders SrFe2S2O and SrFe2Se2O As Probed by Neutron Diffraction and Mössbauer Spectroscopy, European Journal of Inorganic Chemistry **2017**, 3829 (2017).

[59] H. WEITZEL, Kristallstrukturverfeinerung von Wolframiten und Columbiten, Zeitschrift für Kristallographie - Crystalline Materials **144**, 238 (1976).

[60] L. C. Bartel and B. Morosin, Exchange Striction in NiO, Phys. Rev. B **3**, 1039 (1971).

[61] M. M. R. Costa, J. A. Paixão, M. J. M. de Almeida, and L. C. R. Andrade, Charge densities of two rutile structures: NiF_2 and CoF_2, Acta Crystallographica Section B **49**, 591 (1993).

[62] A. Adam, D. Billerey, C. Terrier, R. Mainard, L. Regnault, J. Rossat-Mignod, and P. Mériel, Neutron diffraction study of the commensurate and incommensurate magnetic structures of NiBr2, Solid State Communications **35**, 1 (1980).

[63] S. Yano, D. Louca, J. Yang, U. Chatterjee, D. E. Bugaris, D. Y. Chung, L. Peng, M. Grayson, and M. G. Kanatzidis, Magnetic structure of $NiS_{2-x}Se_x$, Phys. Rev. B **93**, 024409 (2016).

[64] M. A. McGuire, Crystal and magnetic structures in layered, transition metal dihalides and trihalides, Crystals **7**, 10.3390/cryst7050121 (2017).

[65] R. Brec, Review on structural and chemical properties of transition metal phosphorous trisulfides MPS3, Solid State Ionics **22**, 3 (1986).

[66] R. Brec, G. Ouvrard, A. Louisy, and J. Rouxel, Proprietes structurales de phases M(II)PX3 (X = S, Se), Annales de Chimie (Paris) (Vol=Year) **5**, 499 (1980).

[67] V. Scatturin, L. Corliss, N. Elliott, and J. Hastings, Magnetic structures of $3d$ transition metal double fluorides, $KMeF_3$, Acta Crystallographica **14**, 19 (1961).

[68] R. O. Keeling, The structure of NiWO4, Acta Crystallographica **10**, 209 (1957).

[69] J. Rodriguez-Carvajal, M. T. Fernandez-Diaz, and J. L. Martinez, Neutron diffraction study on structural and magnetic properties of La2NiO4, Journal of Physics: Condensed Matter **3**, 3215 (1991).

[70] Plumier, R. and Legrand, E., Structure magnétique de K2NiF4, J. Phys. Radium **23**, 474 (1962).

[71] M. Lujan, J.-P. Rivera, S. Kizhaev, H. Schmid, G. Triscone, J. Muller, Z.-G. Ye, B. Mettout, and R. Bouzerar, Magnetic measurements and magnetoelectric effect of pyroelectric KNiPO4 single crystals, Ferroelectrics **161**, 77 (1994).

[72] I. Abrahams and K. S. Easson, Structure of lithium nickel phosphate, Acta Crystallographica Section C **49**, 925 (1993).

[73] J. B. Forsyth, P. J. Brown, and B. M. Wanklyn, Magnetism in cupric oxide, Journal of Physics C: Solid State Physics **21**, 2917 (1988).

[74] P. Fischer, W. Hälg, D. Schwarzenbach, and H. Gamsjäger, Magnetic and crystal structure of copper(II) fluoride, Journal of Physics and Chemistry of Solids **35**, 1683 (1974).

[75] V. Blum, R. Gehrke, F. Hanke, P. Havu, V. Havu, X. Ren, K. Reuter, and M. Scheffler, Ab initio molecular simulations with numeric atom-centered orbitals, Computer Physics Communications **180**, 2175 (2009).

[76] See Supplemental Material at URL-will-be-inserted-by-publisher for additional data.

[77] S. L. Dudarev, G. A. Botton, S. Y. Savrasov, C. J. Humphreys, and A. P. Sutton, Electron-energy-loss spectra and the structural stability of nickel oxide: An lsda+u study, Phys. Rev. B **57**, 1505 (1998).

[78] I. Timrov, N. Marzari, and M. Cococcioni, Hubbard parameters from density-functional perturbation theory, Phys. Rev. B **98**, 085127 (2018).

[79] I. Timrov, N. Marzari, and M. Cococcioni, Self-consistent hubbard parameters from density-functional perturbation theory in the ultrasoft and projector-augmented wave formulations, Phys. Rev. B **103**, 045141 (2021).

[80] M. Reehuis, C. Ulrich, P. Pattison, B. Ouladdiaf, M. C. Rheinstädter, M. Ohl, L. P. Regnault, M. Miyasaka, Y. Tokura, and B. Keimer, Neutron diffraction study of YVO_3, $NdVO_3$, and $TbVO_3$, Phys. Rev. B **73**, 094440 (2006).

[81] H. Holseth, A. Kjekshus, A. F. Andresen, L. Schäfer, and A. Shimizu, Compounds with the Marcasite Type Crystal Structure. VI. Neutron Diffraction Studies of CrSb2 and FeSb2., Acta Chemica Scandinavica **24**, 3309 (1970).

[82] B. C. Sales, A. F. May, M. A. McGuire, M. B. Stone, D. J. Singh, and D. Mandrus, Transport, thermal, and magnetic properties of the narrow-gap semiconductor $CrSb_2$, Phys. Rev. B **86**, 235136 (2012).

[83] J. W. Stout and R. C. Chisholm, Heat Capacity and Entropy of CuCl2 and CrCl2 from 11° to 300°K. Magnetic Ordering in Linear Chain Crystals, The Journal of Chemical Physics **36**, 979 (1962).

[84] M. Winkelmann, M. Baehr, M. Reehuis, M. Steiner, M. Hagiwara, and K. Katsumata, Structural and magnetic characterization of a new phase of CrCl2, Journal of Physics and Chemistry of Solids **58**, 481 (1997).

[85] J. W. Cable, M. K. Wilkinson, and E. O. Wollan, Neutron Diffraction Studies of Antiferromagnetism in CrF_2 and $CrCl_2$, Phys. Rev. **118**, 950 (1960).

[86] T. Chatterji and T. C. Hansen, Magnetoelastic effects in Jahn–Teller distorted CrF2 and CuF2 studied by neutron powder diffraction, Journal of Physics: Condensed Matter **23**, 276007 (2011).

[87] E. Samuelsen, M. Hutchings, and G. Shirane, Inelastic neutron scattering investigation of spin waves and magnetic interactions in Cr2O3, Physica **48**, 13 (1970).

[88] B. N. Brockhouse, Antiferromagnetic Structure in Cr2O3, The Journal of Chemical Physics **21**, 961 (1953).

[89] M. Fiebig, D. Fröhlich, and H. J. Thiele, Determination of spin direction in the spin-flop phase of Cr_2O_3, Phys. Rev. B **54**, R12681 (1996).

[90] E. J. Telford, A. H. Dismukes, K. Lee, M. Cheng, A. Wieteska, A. K. Bartholomew, Y.-S. Chen, X. Xu, A. N. Pasupathy, X. Zhu, C. R. Dean, and X. Roy, Layered Antiferromagnetism Induces Large Negative Magnetoresistance in the van der Waals Semiconductor CrSBr, Advanced Materials **32**, 2003240 (2020).

[91] M. Zhu, M. Matsumoto, M. B. Stone, Z. L. Dun, H. D. Zhou, T. Hong, T. Zou, S. D. Mahanti, and X. Ke, Amplitude modes in three-dimensional spin dimers away from quantum critical point, Phys. Rev. Res. **1**, 033111 (2019).

[92] M. Kohgi, Y. Ishikawa, and Y. Endoh, Inelastic neutron scattering study of spin waves in MnO, Solid State Communications **11**, 391 (1972).

[93] M. J. Grzybowski, C. Autieri, J. Domagala, C. Krasucki, A. Kaleta, S. Kret, K. Gas, M. Sawicki, R. Bożek, J. Suffczyński, and W. Pacuski, Wurtzite vs. rock-salt mnse epitaxy: electronic and altermagnetic properties, Nanoscale **16**, 6259 (2024).

[94] R. J. Pollard, V. H. McCann, and J. B. Ward, Magnetic structures of α-MnS and MnSe from 57Fe Mossbauer spectroscopy, Journal of Physics C: Solid State Physics **16**, 345 (1983).

[95] E. Uchida, H. Kondoh, and N. Fukuoka, Magnetic and Electrical Properties of Manganese Telluride, Journal of the Physical Society of Japan **11**, 27 (1956).

[96] W. Szuszkiewicz, E. Dynowska, B. Witkowska, and B. Hennion, Spin-wave measurements on hexagonal MnTe of NiAs-type structure by inelastic neutron scattering, Phys. Rev. B **73**, 104403 (2006).

[97] N. Ohama and Y. Hamaguchi, Determination of the Exchange Integrals in β-MnO2, Journal of the Physical Society of Japan **30**, 1311 (1971).

[98] H. Sato, K. Wakiya, T. Enoki, T. Kiyama, Y. Wakabayashi, H. Nakao, and Y. Murakami, Magnetic Structure of β-MnO 2: X-ray Magnetic Scattering Study, Journal of the Physical Society of Japan **70**, 37 (2001).

[99] P. Nordblad, L. Lundgren, E. Figueroa, and O. Beckman, Specific heat and magnetic susceptibility of MnF2 and Mn0.98Fe0.02F2 near TN, Journal of Magnetism and Magnetic Materials **23**, 333 (1981).

[100] N. Akutsu and H. Ikeda, Specific Heat Capacities of CoF_2, MnF_2 and $KMnF_3$ near the Néel Temperatures, Journal of the Physical Society of Japan **50**, 2865 (1981).

[101] T. Chattopadhyay, T. Brückel, and P. Burlet, Spin correlation in the frustrated antiferromagnet MnS_2 above the Néel temperature, Phys. Rev. B **44**, 7394 (1991).

[102] T. Chattopadhyay, H. Schnering, and H. Graf, First order antiferromagnetic phase transition in MnS2, Solid State Communications **50**, 865 (1984).

[103] J. Westrum, Edgar F. and F. Gro/nvold, Manganese Disulfide (Hauerite) and Manganese Ditelluride. Thermal Properties from 5 to 350°K and Antiferromagnetic Transitions, The Journal of Chemical Physics **52**, 3820 (1970).

[104] M. Pasternak, Magnetization near an iodine impurity in antiferromagnetic $mnte_2$, Phys. Rev. **184**, 523 (1969).

[105] J. Greedan, N. Raju, and I. Davidson, Long Range and Short Range Magnetic Order in Orthorhombic LiMnO2, Journal of Solid State Chemistry **128**, 209 (1997).

[106] D. Kellerman, J. Medvedeva, V. Gorshkov, A. Kurbakov, V. Zubkov, A. Tyutyunnik, and V. Trunov, Structural and magnetic properties of orthorhombic LixMnO2, Solid State Sciences **9**, 196 (2007).

[107] P. Battle, T. Gibb, and C. Jones, The structural and magnetic properties of SrMnO3: A reinvestigation, Journal of Solid State Chemistry **74**, 60 (1988).

[108] A. Okazaki and Y. Suemune, The Crystal Structures of KMnF3, KFeF3, KCoF3, KNiF3 and KCuF3 above and below their Néel Temperatures, Journal of the Physical Society of Japan **16**, 671 (1961).

[109] K. Hirakawa, K. Hirakawa, and T. Hashimoto, Magnetic Properties of Potassium Iron Group Fluorides KMF_3, Journal of the Physical Society of Japan **15**, 2063 (1960).

[110] Y. Suemune and H. Ikawa, Thermal Conductivity of KMnF3, KCoF3, KNiF3, and KZnF3 Single Crystals, Journal of the Physical Society of Japan **19**, 1686 (1964).

[111] S. Ogawa, Antiferromagnetism in $KMnF_3$, Journal of the Physical Society of Japan **14**, 1115 (1959).

[112] G. Le Flem, R. Brec, G. Ouvard, A. Louisy, and P. Segransan, Magnetic interactions in the layer compounds MPX3 (M = Mn, Fe, Ni; X = S, Se), Journal of Physics and Chemistry of Solids **43**, 455 (1982).

[113] P. A. Joy and S. Vasudevan, Magnetism in the layered transition-metal thiophosphates MPS_3 (M=Mn, Fe, and Ni), Phys. Rev. B **46**, 5425 (1992).

[114] A. Wiedenmann, J. Rossat-Mignod, A. Louisy, R. Brec, and J. Rouxel, Neutron diffraction study of the layered compounds MnPSe3 and FePSe3, Solid State Communications **40**, 1067 (1981).

[115] J. M. Mays, Nuclear Magnetic Resonances and Mn-O-P-O-Mn Superexchange Linkages in Paramagnetic and Antiferromagnetic $LiMnPO_4$, Phys. Rev. **131**, 38 (1963).

[116] S. Gnewuch and E. E. Rodriguez, Distinguishing the Intrinsic Antiferromagnetism in Polycrystalline $LiCoPO_4$ and $LiMnPO_4$ Olivines, Inorganic Chemistry **59**, 5883 (2020), epub 2020 Apr 22.

[117] D. Arčon, A. Zorko, R. Dominko, and Z. Jagličič, A comparative study of magnetic properties of LiFePO4 and LiMnPO4, Journal of Physics: Condensed Matter **16**, 5531 (2004).

[118] J. Li, W. Tian, Y. Chen, J. L. Zarestky, J. W. Lynn, and D. Vaknin, Antiferromagnetism in the magnetoelectric effect single crystal $LiMnPO_4$, Phys. Rev. B **79**, 144410 (2009).

[119] P. Gilad, M. Greenshpan, P. Hillman, and H. Shechter, On the curie temperature of α-fe2o3, Physics Letters **7**, 239 (1963).

[120] L. Oravova, Z. Zhang, N. Church, R. J. Harrison, C. J. Howard, and M. A. Carpenter, Elastic and anelastic relaxations accompanying magnetic ordering and spin-flop transitions in hematite, Fe2O3, Journal of Physics: Condensed Matter **25**, 116006 (2013).

[121] F. J. Morin, Magnetic Susceptibility of αFe_2O_3 and αFe_2O_3 with Added Titanium, Phys. Rev. **78**, 819 (1950).

[122] Nešković, N. B. and Babić, B. and Konstantinović, J., High temperature anomalous behaviour of the crystal lattice of hematite, physica status solidi (a) **41**, K133 (1977).

[123] M. Białek, J. Zhang, H. Yu, and J.-P. Ansermet, Antiferromagnetic resonance in α-Fe2O3 up to its Néel temperature, Applied Physics Letters **121**, 032401 (2022).

[124] I. Sosnowska, T. P. Neumaier, and E. Steichele, Spiral magnetic ordering in bismuth ferrite, Journal of Physics C: Solid State Physics **15**, 4835 (1982).

[125] P. Fischer, M. Polomska, I. Sosnowska, and M. Szymanski, Temperature dependence of the crystal and magnetic structures of BiFeO3, Journal of Physics C: Solid State Physics **13**, 1931 (1980).

[126] W. Koehler and E. Wollan, Neutron-diffraction study of the magnetic properties of perovskite-like compounds LaBO3, Journal of Physics and Chemistry of Solids **2**, 100 (1957).

[127] K. Park, H. Sim, J. C. Leiner, Y. Yoshida, J. Jeong, S. ichiro Yano, J. Gardner, P. Bourges, M. Klicpera, V. Sechovský, M. Boehm, and J.-G. Park, Low-energy spin dynamics of orthoferrites AFeO3 (A=Y, La, Bi), Journal of Physics: Condensed Matter **30**, 235802 (2018).

[128] H. Shen, J. Xu, A. Wu, J. Zhao, and M. Shi, Magnetic and thermal properties of perovskite YFeO3 single crystals, Materials Science and Engineering: B **157**, 77 (2009).

[129] K. C. Rule, G. J. McIntyre, S. J. Kennedy, and T. J. Hicks, Single-crystal and powder neutron diffraction experiments on $FePS_3$: Search for the magnetic structure, Phys. Rev. B **76**, 134402 (2007).

[130] J. T. Dehn, R. E. Newnham, and L. N. Mulay, Mixed Magnetic Ordering: Magnetic Susceptibility and Mössbauer Studies on Iron(III) Tellurate (Fe2TeO6), The Journal of Chemical Physics **49**, 3201 (1968).

[131] M. Yamaguchi and M. Ishikawa, Magnetic Phase Transitions in Inverse Trirutile-Type Compounds, Journal of the Physical Society of Japan **63**, 1666 (1994).

[132] S. Buksphan, E. Fischer, and R. Hornreich, Magnetoelectric and Mössbauer studies of Fe2TeO6, Solid State Communications **10**, 657 (1972).

[133] S. Huh, Y. Prots, P. Adler, L. H. Tjeng, and M. Valldor, Synthesis and Characterization of Frustrated Spin Ladders SrFe2S2O and SrFe2Se2O, European Journal of Inorganic Chemistry **2015**, 2982 (2015).

[134] J. Deng, L. Chang, P. Wang, E. Zhang, J. Ma, and T. Wang, Preparation and magnetic properties of CoWO4 nanocrystals, Crystal Research and Technology **47**, 1004 (2012).

[135] J. R. Tomlinson, L. Domash, R. G. Hay, and C. W. Montgomery, The High Temperature Heat Content of Nickel Oxide, Journal of the American Chemical Society **77**, 909 (1955).

[136] A. H. Cooke, K. A. Gehring, and R. Lazenby, The magnetic properties of NiF2, Proceedings of the Physical Society **85**, 967 (1965).

[137] P. A. Fleury, Paramagnetic spin waves and correlation functions in nif_2, Phys. Rev. **180**, 591 (1969).

[138] P. Day, A. Dinsdale, E. R. Krausz, and D. J. Robbins, Optical and neutron diffraction study of the magnetic phase diagram of NiBr2, Journal of Physics C: Solid State Physics **9**, 2481 (1976).

[139] R. H. Busey and W. F. Giauque, The Heat Capacity of Anhydrous NiCl2 from 15 to 300°K. The Antiferromagnetic Anomaly near 52°K. Entropy and Free En-

ergy1, Journal of the American Chemical Society **74**, 4443 (1952).

[140] P. A. Lindgard, R. J. Birgeneau, H. J. Guggenheim, and J. Als-Nielsen, Spin-wave dispersion and sublattice magnetization in NiCl2, Journal of Physics C: Solid State Physics **8**, 1059 (1975).

[141] M. A. Prosnikov, V. Y. Davydov, A. N. Smirnov, M. P. Volkov, R. V. Pisarev, P. Becker, and L. Bohatý, Lattice and spin dynamics in a low-symmetry antiferromagnet $NiWO_4$, Phys. Rev. B **96**, 014428 (2017).

[142] K. Nakajima, K. Yamada, S. Hosoya, T. Omata, and Y. Endoh, Spin-Wave Excitations in Two Dimensional Antiferromagnet of Stoichiometric La2NiO4, Journal of the Physical Society of Japan **62**, 4438 (1993).

[143] R. J. Birgeneau, J. Skalyo, J., and G. Shirane, Phase Transitions and Magnetic Correlations in Two-Dimensional Antiferromagnets, Journal of Applied Physics **41**, 1303 (1970).

[144] M. B. Salamon and H. Ikeda, Specific Heat of Two-Dimensional Heisenberg Antiferromagnets: K_2MnF_4 and K_2NiF_4, Phys. Rev. B **7**, 2017 (1973).

[145] E. Legrand and R. Plumier, Neutron diffraction investigation of antiferromagnetic K2NiF4, physica status solidi (b) **2**, 317 (1962).

[146] A. Pages, J.-R. Soh, M. J. Fesharaki, H. M. Ronnow, and H. Ahmadvand, Revisiting the magnetic and crystal structure of multiferroic $KNiPO_4$ (2022), arXiv:2207.06969.

[147] Y. N. Kharchenko, N. F. Kharcheno, M. Baran, and R. Szymczak, Weak ferromagnetism and an intermediate incommensurate antiferromagnetic phase in LiNiPO4, Low Temperature Physics **29**, 579 (2003).

[148] D. Vaknin, J. L. Zarestky, J.-P. Rivera, and H. Schmid, Commensurate-Incommensurate Magnetic Phase Transition in Magnetoelectric Single Crystal $LiNiPO_4$, Phys. Rev. Lett. **92**, 207201 (2004).

[149] J.-H. Hu and H. L. Johnston, Low Temperature Heat Capacities of Inorganic Solids. XVI. Heat Capacity of Cupric Oxide from 15 to 300 °K.1, Journal of the American Chemical Society **75**, 2471 (1953).

[150] B. X. Yang, J. M. Tranquada, and G. Shirane, Neutron scattering studies of the magnetic structure of cupric oxide, Phys. Rev. B **38**, 174 (1988).

[151] R. J. Joenk and R. M. Bozorth, Magnetic properties of cuf2, Journal of Applied Physics **36**, 1167 (1965).